Preprints of the 19th World Congress
The International Federation of Automatic Control
Cape Town, South Africa. August 24-29, 2014

Experimental Comparison of Sensor Fusion Algorithms for Attitude Estimation

A. Cavallo, A. Cirillo, P. Cirillo, G. De Maria, P. Falco, C. Natale, S. Pirozzi

Dipartimento di Ingegneria Industriale e dell'Informazione, Seconda Università degli Studi di Napoli, Via Roma 29, 81031 Aversa, Italy (e-mail: andrea.cirillo@unina2.it).

Abstract: Inertial Measurement Unit is commonly used in various applications especially as a low-cost system for localization and attitude estimation. Some applications are: real-time motion capture system, gait analysis for rehabilitation purposes, biomedical applications, advanced robotic applications such as mobile robot localization and Unmanned Aerial Vehicles (UAV) attitude estimation. In all the mentioned applications the accuracy and the fast response are the most important requirements, thus the research is focused on the design and the implementation of highly accurate hardware systems and fast sensor data fusion algorithms, named Attitude and Heading Reference System (AHRS), aimed at estimating the orientation of a rigid body with respect to a reference frame. A large number of different solutions can be found in the literature, and an experimental comparison of the most popular is presented in this work. In particular, the algorithm based on the gradient descent method and the algorithm based on a nonlinear complementary filter are compared to a standard Extended Kalman Filter (EKF) with the aim to show that a general method can easily compete with ad-hoc solutions and even outperform them in particular conditions. In order to validate the estimation accuracy a Kuka robot is used to compute the ground truth. Moreover, in order to estimate the computational burden, the algorithms are implemented on an ARM-Cortex M4-based evaluation board.

Keywords: Sensor fusion, Extended Kalman Filter, Advanced Robotics, Attitude estimation

1. INTRODUCTION

Inertial Measurement Unit (IMU) sensors are a technology capable of estimating orientation of a rigid body so they are largely used as an implementation of real-time motion capture systems to track the location and the body posture of people (see Ziegler et al. (2011), Prayudi and Doik (2012)) in contrast to optical solutions such as (Falco et al., 2012), or to measure the joint angles for gait analysis for rehabilitation purposes and biomedical applications as well as for performance assessment of the aging population (see Zecca et al. (2013) and Bennett et al. (2013). Also, because of the small size and low weight that make it better suited to the purpose, the interest for IMU-based systems is growing in advanced robotic applications, i.e., localization and wheel slip estimation of a skid steered mobile robot (Jingang et al. (2007)), position and attitude determination for unmanned airborne vehicles (UAVs) (Joong-hee et al. (2011)) and unmanned underwater vehicles (UUVs) (Kim et al. (2011)). In all these applications, in order to provide an added value and to provide a valid alternative to the typical expensive tools such as optical camera track systems, high accuracy and high precision estimation of the device orientation are required. So, the research is focusing on the design and the implementation of sensor data fusion algorithms, named Attitude and Heading Reference System (AHRS), able to estimate the orientation of a rigid body with respect to a reference frame. The IMU provides real-time readings of a tri-axial gyroscope and a tri-axial accelerometer, which can be employed in orientation estimation. The signal output of low-cost IMU systems, however, is characterized by low-resolution signals subject to high noise levels as well as general time-varying bias terms. Therefore, raw signals must be processed to reconstruct smoothed attitude estimates and bias-corrected angular velocity measurements through suitable sensor fusion algorithms. In fact, suitable exploitation of acceleration measurements can avoid drift caused by numerical integration of gyroscopic measurements. However, it is well-known that use of only these two source of information cannot correct the drift of the estimated heading, thus an additional sensor is needed, i.e., a tri-axial compass, which allows to obtain a correct heading estimation. Several fusion methods have been proposed in the literature. Mahony et al. (2008) formulate the filtering problem as a deterministic observer posed on the special orthogonal group $SO(3)$ termed 'explicit complementary filter'. Madgwick et al. (2011) present a computationally efficient orientation algorithm based on optimized gradient descent algorithm designed to support a wearable inertial human motion tracking system for rehabilitation applications.

The contribution of this paper is to experimentally compare the most popular AHRS algorithms and to validate them using a robotic manipulator in order to define a reliable ground truth. In particular, the standard EKF framework and the methods proposed by Mahony et al.

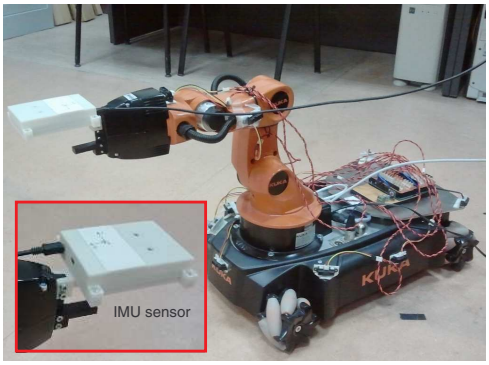

Fig. 1. Experimental setup.

(2008) and by Madgwick et al. (2011) have been considered worthy of particular interest. Although most of the papers in literature propose modified versions of the EKF, e.g. (Kim et al., 2011), (Chen et al., 2012) and (Xia et al., 2008), the authors consider the standard EKF framework still a valid option. The main reasons are its generality and flexibility. In fact, this framework is particularly suitable to add and remove sensors without significantly changing the estimation algorithm, to take into account the different reliability and accuracy of sensors on the basis of their statistical characteristics, and to easily exploit all the a priori knowledge on the involved signals.

In the first phase, the AHRS algorithms are implemented in Matlab/Simulink environment. The IMU is then mounted on a KUKA robot by mechanically aligning the sensor frame to the end-effector frame. The gyroscope, accelerometer, magnetometer and joint angles of the robot are simultaneously acquired. By computing the direct kinematics of the robot, the orientation of the end-effector frame can be obtained. Thus, the estimated orientation and the accuracy of the AHRS algorithms can be validated using the measured orientation. In the second phase, in order to compare the computational burden of the AHRS algorithms, they are implemented on an embedded system constituted by an ARM-Cortex M4. In this case, the required time to compute a single cycle of data sensor acquisition and filter computation is measured.

2. EXPERIMENTAL SETUP

The experimental setup is constituted by a KUKA robot and by a STM32F3Discovery board. The evaluation board is based on the STM32F303VCT6 ARM-Cortex M4 microcontroller, a ST L3GD20 3-axis digital output gyroscope, a ST LSM303DLHC MEMS system-in-package featuring a 3D digital linear acceleration sensor and a 3D digital magnetic sensor. In order to mechanically align the sensor frame to the robot end-effector frame and in order to avoid undesired rotations, the evaluation board is fixed to the robot gripper using a calibrated mechanical part. In Fig 1 the experimental setup is reported.

2.1 IMU

The considered IMU is constituted by ST MEMS motion sensors directly mounted on the STM32F3Discovery evaluation board. The ST L3GD20 3-axis gyroscope offers an I2C/SPI digital output interface, 16 bit value data output and three selectable ranges (± 250, ± 500, ± 2000 dps) while the ST LSM303DLHC offers a 3-axis magnetometer with a full-scale from ± 1.3 to ± 8.1 Gauss and a 3-axis accelerometer with $\pm 2\,g/\pm 4\,g/\pm 8\,g/\pm 16\,g$ selectable range, 16 bit data output and a I2C serial interface. The experiments have been carried out by setting an acquisition rate of 760 Hz, 1344 Hz, 220 Hz and a full-scale range of ± 2000 dps, $\pm 2\,g$, ± 1.3 Gauss for the gyroscope, the accelerometer and the magnetometer, respectively.

2.2 Robot

The robot used to compute the ground truth for performing the comparison among the attitude estimation algorithms is a KUKA Youbot (Bischoff et al., 2011) constituted by a 5-dof serial manipulator mounted on an omnidirectional platform. In order to obtain a reference attitude with a clear geometrical interpretation, the first phase of the planned trajectory consists of rotating the three joints with orthogonal axes of the robot individually, while, in the second phase the joints are moved in a coordinated fashion so as generate rotations about the roll, pitch and yaw axes contemporarily. The joint angle values are measured using the robot encoders with a sampling frequency of 40 Hz.

3. SENSOR CALIBRATION

Low-cost sensors have much lower performance characteristics than high-end sensors for sophisticated applications. Therefore, an accurate calibration of such sensors is very important for the compensation of their systematic errors, i.e., bias and scale factor. Usually, accurate values of such parameters are not available from the manufacturer or they depend on the actual mounting of the MEMS components, which limits the use of these sensors for those applications that require high accuracy, such as human-machine interfaces, biomedical research and aerial robotics. To obtain a satisfactory performance, it is necessary to use a proper calibration method that could be performed in the background (self-calibration) or off-line by the system.

Three-axis accelerometers and three-axis magnetometers supplied for the consumer market are typically calibrated by the sensor manufacturer using a six-element linear model comprising a gain and offset in each of the three axes. This factory calibration can change as a result of the thermal stresses during soldering of the accelerometer/magnetometer to the circuit board. Additional small errors, including rotation of the IC package relative to the circuit board and misalignment of the circuit board to the final product, can be introduced during the soldering and final assembly process. The original factory calibration will still be adequate for the vast majority of applications, however for professional applications this is not the case. In addition, the magnetometer behaviour can be influenced by the presence of hard-iron and soft-iron distortions that cannot be foreseen by the manufactures but are strictly related to the application. Hard-iron interference is normally generated by ferromagnetic materials with permanent magnetic fields that are part of the hand-held device structure. These materials could be permanent magnets or magnetized iron or steel. They are time invariant and their

effect is to bias the magnetic sensor outputs. A soft-iron interference magnetic field is generated by the items inside the hand-held device. They could be the electric traces on the PCB or other magnetically soft materials.

3.1 Accelerometer/Magnetometer Calibration

Calibration of accelerometers and magnetometers can be reduced to 3D-ellipsoid fitting problems (Gietzelt et al., 2013), (Camps et al., 2009). In the proposed calibration algorithm a six-parameter error model has been considered (Pedley, 2013). Denoting with $\boldsymbol{y}_f = [y_{f1}\ \ y_{f2}\ \ y_{f3}]^T$ a generic sensor output, a re-calibration procedure can be applied to compute the same six calibration parameters as the original factory calibration (a scale factor and an offset for each channel) but then applied on top of the factory calibrated output $\boldsymbol{y}_f$. The 3D fitting problem requires a set of measurements that should cover as much as possible the 3D space and, for the accelerometer calibration, it is necessary to carry out the measurements in a quasi-static condition to avoid accelerations other than the gravity. The re-calibrated sensor output $\hat{\boldsymbol{y}}^s$, expressed in the sensor frame Σ_s, become

$$\hat{\boldsymbol{y}}^s = \boldsymbol{\Lambda}\left(\boldsymbol{y}_f^s - \boldsymbol{b}^s\right) = \boldsymbol{\Lambda}\boldsymbol{y}_f^s - \boldsymbol{\Lambda}\boldsymbol{b}^s \tag{1}$$

where $\boldsymbol{\Lambda} = \text{diag}\{\lambda_1, \lambda_2, \lambda_3\} > 0$ and $\boldsymbol{b}^s = [b_1\ \ b_2\ \ b_3]^T$ are the scale factors and offsets, respectively.

Objective of the calibration is to compute $\boldsymbol{\Lambda}$ and $\boldsymbol{b}$ such that the ellipsoid becomes a unit sphere centered in the origin, i.e.,

$$1 = \hat{\boldsymbol{y}}^{s^T}\hat{\boldsymbol{y}}^s = \boldsymbol{y}_f^{s^T}\boldsymbol{\Lambda}^2\boldsymbol{y}_f^s + \boldsymbol{b}^{s^T}\boldsymbol{\Lambda}^2\boldsymbol{b}^s - 2\boldsymbol{y}_f^{s^T}\boldsymbol{\Lambda}^2\boldsymbol{b}^s \tag{2}$$

By introducing the following intermediate variables [1]

$$d = 1 - \boldsymbol{b}^{s^T}\boldsymbol{\Lambda}^2\boldsymbol{b}^s \tag{3}$$

$$\bar{\boldsymbol{\Lambda}} = (1/d)\boldsymbol{\Lambda}^2 = \text{diag}\{\bar{\lambda}_1, \bar{\lambda}_2, \bar{\lambda}_3\} \tag{4}$$

$$\boldsymbol{c} = (1/d)\boldsymbol{\Lambda}^2\boldsymbol{b}^s = \bar{\boldsymbol{\Lambda}}\boldsymbol{b}^s, \tag{5}$$

Eq. (2) can be written as

$$1 = \begin{bmatrix} y_{f1}^2 & y_{f2}^2 & y_{f3}^2 - 2y_{f1} - 2y_{f2} - 2y_{f3} \end{bmatrix} \begin{bmatrix} \bar{\lambda}_1 \\ \bar{\lambda}_2 \\ \bar{\lambda}_3 \\ \boldsymbol{c} \end{bmatrix}, \tag{6}$$

which can be easily solved by writing it for the entire measurement set as a linear system to be solved via a least square algorithm. The bias term $\boldsymbol{b}^s$ can be immediately computed from (5), while $\boldsymbol{\Lambda}^2$ can be computed by solving the linear system obtained substituting Eq. (3) into (4).

The algorithm has been applied to both the magnetometer and the accelerometer of the IMU used in the experimental setup and the results are reported in Fig. 2, where it is evident how the re-calibration allows to obtain lower errors. In fact, after the re-calibration the standard deviation of $\|\hat{\boldsymbol{y}}^s\|$ is 2.8% for the magnetometer and 3.1% for the accelerometer, compared to the standard deviations of $\|\tilde{\boldsymbol{y}}_f^s\| = \|\boldsymbol{y}_f^s\|/\bar{\boldsymbol{y}}_f^s$ that are 17.9% and 5.2%, respectively, being $\bar{\boldsymbol{y}}_f^s$ the mean value of $\boldsymbol{y}_f^s$.

[1] Note that $d = 0$ can always be avoided by artificially translating the data.

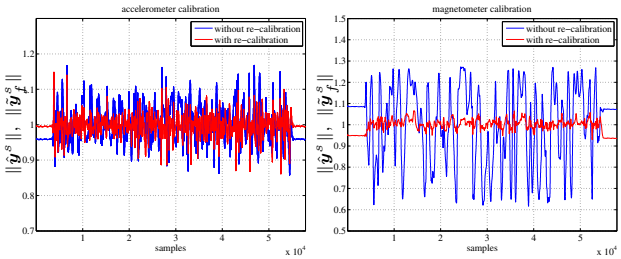

Fig. 2. Calibration error of the accelerometer (left) and magnetometer (right) before and after re-calibration.

4. ATTITUDE ESTIMATION ALGORITHMS

As explained in the introduction, in this work three attitude estimation algorithms have been compared, one based on a standard EKF formulation and two specifically designed to solve the problem. As opposed to what one would expect from a specifically designed solution compared to a more general approach, the performance of the EKF will be demonstrated better than the other two methods, at the price of a higher computational burden. Nevertheless, the generality of the approach keeps the "door open" to further improvements that could come from the adoption of additional sensor data without the need to completely re-design the estimation algorithm and especially re-tune the algorithm parameters, which are based on the statistic characteristics of each signal.

4.1 Extended Kalman Filter

The proposed AHRS algorithm is based on a standard EKF method differently from the Kalman-based approaches proposed in Marins et al. (2001) and Sabatini (2006), where modifications to the standard Bayesian framework were introduced with different motivations. However, the modification proposed by Marins et al. (2001) lead to a solution where handling of noise statistics is less trivial than in the standard EKF formulation, in fact noise rejection is delegated to a Gauss-Newton iterative algorithm, which is claimed less computational demanding than the standard EKF, but without a convincing evidence. The modification proposed by Sabatini (2006) consists in introducing the gyroscopic measurement directly in the state update equation rather than in the measurement equation, which implies the assumption of low noise affecting the sensor so as to allow a linearization of the update function. Finally, the recent survey on nonlinear attitude estimation techniques (Crassidis et al. (2007)) recognizes that EKF-based approaches are the most used for two main reasons, their proven reliability and the ease of incorporation of further measurement sources that can improve the quality of the estimate or even provide estimate of further quantities, e.g. altitude and vertical velocity using GPS, like in Xia et al. (2008). Moreover, the statistical characterization of the sensors required in the EKF framework allows tuning the algorithm parameters in a more straightforward fashion.

Let Σ_b be the base frame to which the orientation to be estimated is referred and Σ_v be the body-fixed frame. Without loss of generality, Σ_v is assumed aligned with the sensor frame Σ_s.

Given two frames Σ_d and Σ_c, the quaternion expressing the orientation of Σ_d with respect to Σ_c is denoted by

$$\boldsymbol{Q}_{d,c} = \begin{bmatrix} q_1^{d,c} & q_2^{d,c} & q_3^{d,c} & q_4^{d,c} \end{bmatrix}^T = \begin{bmatrix} \eta^{d,c} & \boldsymbol{\epsilon}^{d,c^T} \end{bmatrix}^T, \quad (7)$$

where $\eta^{d,c} = q_1^{d,c}$ is the scalar part and $\boldsymbol{\epsilon}^{d,c} = [q_2^{d,c} \; q_3^{d,c} \; q_4^{d,c}]^T$ is the vector part. Note that a quaternion is here represented as a 4×1 vector and two operators can be applied to two quaternions, i.e. the standard matrix product and the quaternion product defined as

$$\boldsymbol{Q}_{d,c} * \boldsymbol{Q}_{e,f} = \begin{bmatrix} \eta^{d,c}\eta^{e,f} - \boldsymbol{\epsilon}^{d,c^T}\boldsymbol{\epsilon}^{d,c} \\ \eta^{d,c}\boldsymbol{\epsilon}^{e,f} + \eta^{e,f}\boldsymbol{\epsilon}^{d,c} + \boldsymbol{S}(\boldsymbol{\epsilon}^{d,c})\boldsymbol{\epsilon}^{e,f} \end{bmatrix}, \quad (8)$$

where $\boldsymbol{S}(\cdot)$ is the 3×3 skew-symmetric operator of the vector product.

In order to simplify the notation, the orientation of Σ_v with respect to Σ_b will be expressed by omitting the frame superscripts, i.e.,

$$\boldsymbol{Q}_{v,b} = [q_1 \; q_2 \; q_3 \; q_4]^T \triangleq \boldsymbol{Q}, \quad (9)$$

which is the quantity to estimate. In order to setup the EKF, the measurement equations are considered first.

Accelerometer. Under the following assumptions

- Σ_b has the z-axis perfectly vertical
- The vehicle is subject to low translational accelerations and thus the accelerometer measures only the gravity acceleration vector
- The accelerometer is calibrated as in Section 3.1 such that $\boldsymbol{a}^{v^T}\boldsymbol{a}^v = 1$ and thus $\boldsymbol{a}^b = [0 \; 0 \; -1]^T$

where $\boldsymbol{a}^v$ is the measured acceleration expressed in the body-fixed frame and $\boldsymbol{a}^b$ is the same acceleration expressed in the base frame, the measurement equation of the accelerometer can be obtained by using the standard quaternion formula to change the reference frame of a vector as

$$\begin{bmatrix} 0 \\ \boldsymbol{a}^v \end{bmatrix} = \boldsymbol{Q}_{v,b}^{-1} * \begin{bmatrix} 0 \\ \boldsymbol{a}^b \end{bmatrix} * \boldsymbol{Q}_{v,b} + \begin{bmatrix} 0 \\ \boldsymbol{n}_a \end{bmatrix} \quad (10)$$

where $\boldsymbol{n}_a$ is the measurement noise affecting acceleration measurements, assumed normally distributed.

Magnetometer. Under the following assumptions

- The magnetometer is calibrated as in Section 3.1 such that $\boldsymbol{h}^{v^T}\boldsymbol{h}^v = 1$
- $\boldsymbol{h}^b$ is constant and is computed as the average value $\bar{\boldsymbol{h}}^b$ measured at the beginning of any experiment

Since the initial orientation (at the time instant $t = 0$) of Σ_v with respect to Σ_b is unknown, but the base frame has been chosen with a vertical z-axis, a rotation matrix $\bar{\boldsymbol{R}}_v^b = \boldsymbol{R}_v^b(0)$ has to be computed to obtain $\bar{\boldsymbol{h}}^b$ from the measurement $\boldsymbol{h}^v(0)$ expressed in frame Σ_v, i.e.,

$$\bar{\boldsymbol{R}}_v^b \boldsymbol{a}^v(0) = [0 \; 0 \; -1]^T \quad (11)$$

where $\boldsymbol{a}^v(0)$ is the measured (averaged) acceleration in $t = 0$. Denoting with

$$\bar{\boldsymbol{R}}_b^v = [\boldsymbol{r}_1 \; \boldsymbol{r}_2 \; \boldsymbol{r}_3], \quad (12)$$

from (11) it results

$$\boldsymbol{r}_3 = -\boldsymbol{a}^v(0), \quad (13)$$

while $\boldsymbol{r}_1$ and $\boldsymbol{r}_2$ can be easily computed to complete a right-handed frame as

$$\boldsymbol{r}_1 = 1/\left\|(\boldsymbol{I} - \boldsymbol{r}_3\boldsymbol{r}_3^T)\boldsymbol{e}_1\right\| (\boldsymbol{I} - \boldsymbol{r}_3\boldsymbol{r}_3^T)\boldsymbol{e}_1 \quad (14)$$

$$\boldsymbol{r}_2 = \boldsymbol{S}(\boldsymbol{r}_1)\boldsymbol{r}_3. \quad (15)$$

Hence, the constant magnetic field in the base frame is computed as $\bar{\boldsymbol{h}}^b = \bar{\boldsymbol{R}}_v^b \boldsymbol{h}^v(0)$ and the measurement equation of the magnetometer is

$$\begin{bmatrix} 0 \\ \boldsymbol{h}^v \end{bmatrix} = \boldsymbol{Q}_{v,b}^{-1} * \begin{bmatrix} 0 \\ \bar{\boldsymbol{h}}^b \end{bmatrix} * \boldsymbol{Q}_{v,b} + \begin{bmatrix} 0 \\ \boldsymbol{n}_m \end{bmatrix}, \quad (16)$$

where $\boldsymbol{n}_m$ is the measurement noise affecting magnetic field measurements, assumed normally distributed.

Gyroscope. The gyroscope provides measurements of the angular velocity, which is related to the time derivative of the quaternion through the equation

$$\dot{\boldsymbol{Q}} = \frac{1}{2}\begin{bmatrix} 0 & -\boldsymbol{\omega}^{v^T} \\ \boldsymbol{\omega}^v & -\boldsymbol{S}(\boldsymbol{\omega}^v) \end{bmatrix} \boldsymbol{Q} \triangleq \boldsymbol{E}(\boldsymbol{\omega}^v)\boldsymbol{Q}. \quad (17)$$

In order to take into account that the angular velocity is affected by an additive measurement noise $\boldsymbol{n}_\omega$ (assumed normally distributed), it will be included both among the measured variables and the variables to be estimated. For implementation purposes, Eq. (17) can be written as a function of the discrete time k as

$$\boldsymbol{Q}_{k+1} = \boldsymbol{Q}_k + T_s\boldsymbol{E}(\boldsymbol{\omega}_k^v)\boldsymbol{Q}_k, \quad (18)$$

where T_s is the sampling time.

Now, the equations of the estimation filter are presented.

The estimation filter. Let us define the augmented state as

$$\boldsymbol{x}_k = \begin{bmatrix} \boldsymbol{x}_{1_k} \\ \boldsymbol{x}_{2_k} \end{bmatrix} = \begin{bmatrix} \boldsymbol{Q}_k \\ \boldsymbol{\omega}_k^v \end{bmatrix}. \quad (19)$$

Assuming the classical constant velocity model, the state update equation is

$$\boldsymbol{x}_{k+1} = \boldsymbol{f}(\boldsymbol{x}_k) + \boldsymbol{w}_k \triangleq \begin{bmatrix} \boldsymbol{x}_{1_k} + T_s\boldsymbol{E}(\boldsymbol{x}_{2_k})\boldsymbol{x}_{1_k} \\ \boldsymbol{x}_{2_k} \end{bmatrix} + \boldsymbol{w}_k \quad (20)$$

where $\boldsymbol{w}_k$ is the process noise which is assumed unbiased, uncorrelated with the state and with a covariance matrix $\boldsymbol{W}$ with finite norm. In order to setup the EKF, the measurement equation is defined as

$$\boldsymbol{y}_k = \begin{bmatrix} \boldsymbol{\omega}_k^v \\ \boldsymbol{a}_k^v \\ \boldsymbol{h}_k^v \end{bmatrix} + \boldsymbol{v}_k = \boldsymbol{g}(\boldsymbol{x}_k) + \boldsymbol{v}_k \triangleq \begin{bmatrix} \boldsymbol{x}_{2_k} \\ \boldsymbol{a}^v(\boldsymbol{x}_{1_k}) \\ \boldsymbol{h}^v(\boldsymbol{x}_{1_k}) \end{bmatrix} + \boldsymbol{v}_k \quad (21)$$

where $\boldsymbol{a}^v(\boldsymbol{x}_{1_k})$ is expressed as in (10), $\boldsymbol{h}^v(\boldsymbol{x}_{1_k})$ is expressed as in (16) and $\boldsymbol{v}_k = [\boldsymbol{n}_\omega^T \; \boldsymbol{n}_a^T \; \boldsymbol{n}_m^T]^T$ is the measurement noise, which is assumed normally distributed and with positive definite covariance matrix $\boldsymbol{V}$.

The EKF equations are set in the classical 3-steps form as

- *prediction step*

$$\hat{\boldsymbol{x}}_{k+1|k} = \boldsymbol{f}(\hat{\boldsymbol{x}}_{k|k}), \qquad \hat{\boldsymbol{x}}_{0|0} = \boldsymbol{x}_i \quad (22)$$

$$\hat{\boldsymbol{P}}_{k+1|k} = \boldsymbol{F}_k\hat{\boldsymbol{P}}_{k|k}\boldsymbol{F}_k^T + \boldsymbol{W}, \quad \hat{\boldsymbol{P}}_{0|0} = \boldsymbol{W} \quad (23)$$

$$\text{being} \quad \boldsymbol{F}_k = \left.\frac{\partial \boldsymbol{f}}{\partial \boldsymbol{x}}\right|_{\hat{\boldsymbol{x}}_{k|k}} \quad (24)$$

- *Kalman gain computation step*

$$\boldsymbol{K}_{k+1} = \hat{\boldsymbol{P}}_{k+1|k}\boldsymbol{G}_{k+1}^{\mathrm{T}}\left(\boldsymbol{G}_{k+1}\hat{\boldsymbol{P}}_{k+1|k}\boldsymbol{G}_{k+1}^{\mathrm{T}} + \boldsymbol{V}\right)^{-1} \quad (25)$$

$$\text{being} \quad \boldsymbol{G}_k = \left.\frac{\partial \boldsymbol{g}}{\partial \boldsymbol{x}}\right|_{\hat{\boldsymbol{x}}_{k+1|k}} \quad (26)$$

- *update step*

$$\hat{\boldsymbol{x}}_{k+1|k+1} = \hat{\boldsymbol{x}}_{k+1|k} + \boldsymbol{K}_{k+1}\left(\boldsymbol{y}_k - \boldsymbol{g}(\hat{\boldsymbol{x}}_{k+1|k})\right) \quad (27)$$

$$\hat{\boldsymbol{P}}_{k+1|k+1} = \left(\boldsymbol{I} - \boldsymbol{K}_{k+1}\boldsymbol{G}_{k+1}\right)\hat{\boldsymbol{P}}_{k+1|k} \quad (28)$$

where $\boldsymbol{x}_i$ is the initial state which is chosen with zero angular velocity and orientation aligned with the base frame, $\boldsymbol{I}$ is the 7×7 identity matrix, $\hat{\boldsymbol{x}}_{k+1|k}$ and $\hat{\boldsymbol{P}}_{k+1|k}$ denote the expected value and covariance matrix estimates, respectively, at time step $k+1$ given the observations up to time step k.

4.2 Madgwick Algorithm

It is applicable to IMU's consisting of tri-axis gyroscopes and accelerometers, and magnetic angular rate and gravity (MARG) sensor arrays that also include tri-axis magnetometers. The algorithm incorporates magnetic distortion compensation and it uses a quaternion representation, allowing accelerometer and magnetometer data to be used in an analytically derived and optimised gradient descent algorithm to compute the direction of the gyroscope measurement error as a quaternion derivative. The equations of the algorithms can be found in Madgwick et al. (2011).

4.3 Non-Linear Complementary Filter

Mahony et al. (2008) propose the orientation estimation problem as a deterministic observation problem posed directly on the special orthogonal group $SO(3)$. Thought the definition of a Direct Complementary Filter and a Passive Complementary Filter they arrive to a reformulation of the complementary filter, named Explicit Complementary Filter, in terms of direct vectorial measurements, such as gravitational or magnetic field directions obtained from an IMU. This observer does not require online algebraic reconstruction of attitude and is ideally suited for implementation on embedded hardware platforms owing to its low complexity. However, it suffers from possible discontinuities in the bias correction signal when the equivalent rotation angle of the estimated quaternion approaches $\pm\pi$ rad that could result in systematic errors in the reconstructed attitude.

5. EXPERIMENTAL RESULTS

The parameters of each of the three algorithms to be compared have been set as follows. For the EKF, the measurement covariance matrix $\boldsymbol{V}$ has been estimated by a simple static acquisition of the sensor signals and the resulting values are

$$\boldsymbol{V} = \text{diag}\{2.9\cdot10^{-5}, 2.3\cdot10^{-5}, 3.2\cdot10^{-5}, 3.1\cdot10^{-5},$$
$$4.5\cdot10^{-5}, 5.5\cdot10^{-5}, 2.0\cdot10^{-3}, 2.1\cdot10^{-3}, 2.0\cdot10^{-3}\}'$$

while the entries of the process covariance matrix have been tuned so as to obtain a satisfactory response time and a good noise rejection, as well as to guarantee filter convergence according to the result by Natale (2011), i.e.,

$$\boldsymbol{W} = \text{diag}\{10^{-10}, 10^{-10}, 10^{-10}, 10^{-10}, 10^{-3}, 10^{-3}, 10^{-3}\}.$$

Note how the first four entries are significantly lower than the others since the first four state update equations in (20) are the kinematic relation between angular velocity and time derivative of the quaternion, which is exact except for the numerical integration error.

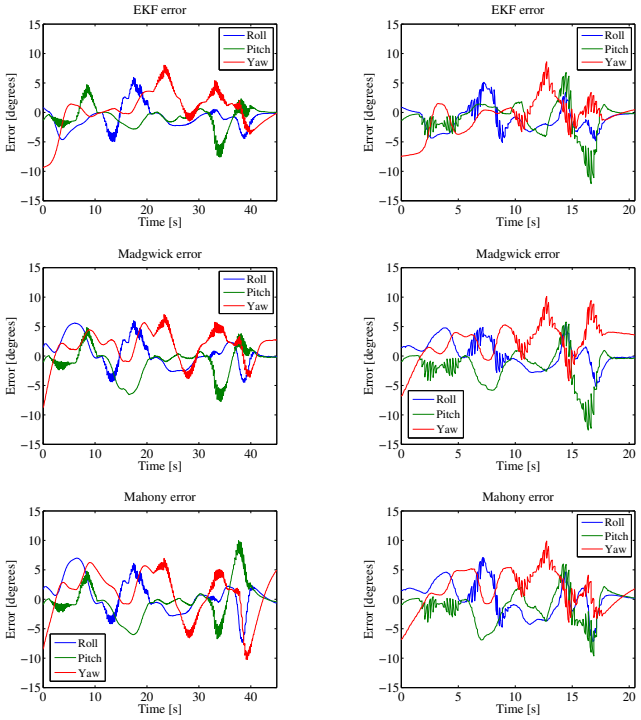

Fig. 3. Orientation error: slow trajectory (left) and fast trajectory (right).

The sole adjustable parameter of the algorithm recalled in Section 4.2 has been chosen as the optimal value proposed by Madgwick et al. (2011) for the MARG implementation, i.e., $\beta = 0.041$. The gain parameters of the algorithm recalled in Section 4.3 and implemented using the quaternion representation, have been chosen as proposed by Mahony et al. (2008), i.e., $K_P = 2$ and $K_I = 0.6$, which have been verified to be optimal also in this case.

The three algorithms have been implemented in Matlab/Simulink with a sampling time $T_s = 2$ ms, since the sensor data have been acquired from IMU at sampling frequency of 500 Hz, which is the frequency experimentally found to guarantee the most reliable communication. To compare the three AHRS algorithms, two robot trajectories are considered. In the first (slow) trajectory, an average speed of 18 deg/s is applied to robot joints, while, in the second (fast) trajectory, the average speed is raised to 45 deg/s. The ground truth is computed using the direct kinematics of the robot and, thus, computing the end-effector frame orientation (aligned to the body-fixed frame) in terms of the unit quaternion $\boldsymbol{Q}_{v,r}$, being Σ_r the robot base frame. Thus, the estimated orientation of the body-fixed frame resulting from the AHRS algorithms $\hat{\boldsymbol{Q}}_{v,b}$, is compared with the ground truth $\boldsymbol{Q}_{v,b}$ (computed as $\boldsymbol{Q}_{v,b}(0) * \boldsymbol{Q}_{r,v}(0) * \boldsymbol{Q}_{v,r}(t)$) and the orientation error is calculated as the quaternion $\tilde{\boldsymbol{Q}}(t) = \hat{\boldsymbol{Q}}^{-1}_{v,b}(t) * \boldsymbol{Q}_{v,b}(t)$. This orientation error is then expressed in terms of Euler angles in Roll-Pitch-Yaw representation and it is reported in Fig. 3.

To better appreciate the response time and noise rejection of the three algorithms, Fig. 4 shows the quaternion

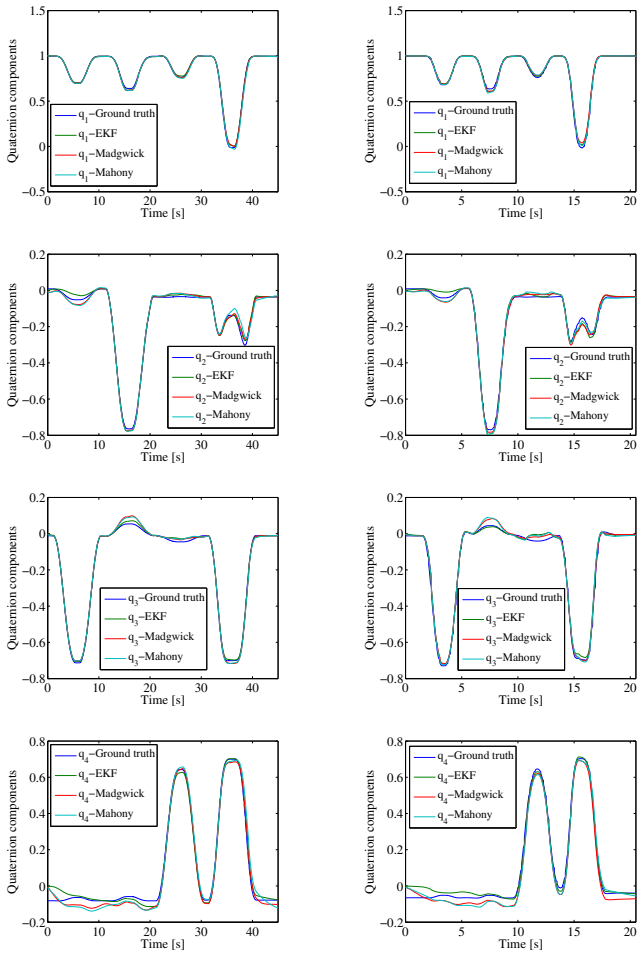

Fig. 4. Estimated and true attitude: slow trajectory (left) and fast trajectory (right).

Euler angles [°]	EKF	Madgwick	Mahony
Roll (static)	0.04	0.03	0.02
Pitch (static)	0.01	0.05	0.05
Yaw (static)	0.30	1.92	1.85
Roll (slow)	4.71	4.85	5.07
Pitch (slow)	1.91	2.65	2.89
Yaw (slow)	5.19	5.13	5.67
Roll (fast)	6.55	6.51	6.69
Pitch (fast)	2.83	3.34	2.85
Yaw (fast)	6.71	7.07	6.92

Table 1. Static and dynamic RMSE

components of the estimated orientation for both trajectories compared to the ground truth. To quantify the algorithms performance, the static and dynamic RMSE (root-mean-square-error) still in terms of Euler angles have been computed and reported in Tab. 1. The results of the experiments show that in the slow trajectory, the three algorithms provide comparable results in terms of accuracy. In terms of RMSE, the proposed EKF algorithm provides a more accurate estimation in both static and dynamic conditions.

To test the capability of the algorithms to work under severe disturbance conditions a specific experiment has been carried out by intentionally actuating the robot gripper with a periodic signal so as to generate an electromagnetic disturbance which mainly affects the magnetometer.

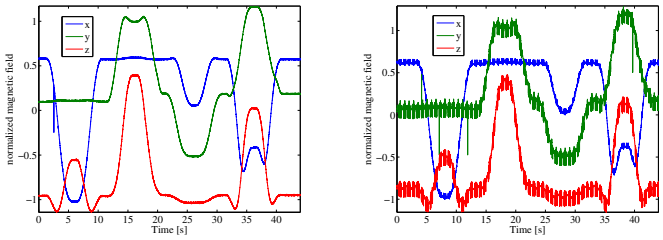

Fig. 5. Measured magnetic field without (left) and with disturbance (right).

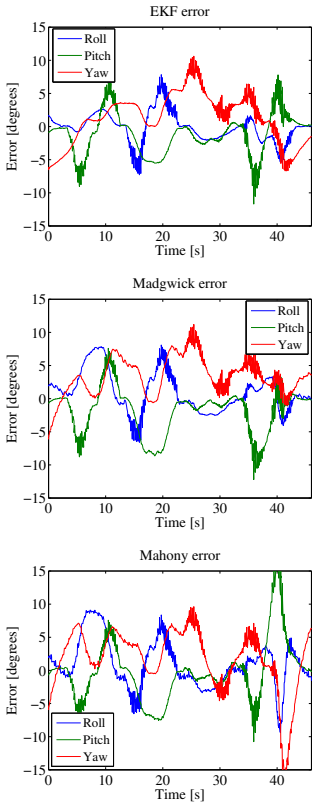

Fig. 6. Orientation error: slow trajectory in the noisy case.

Euler angles [°]	EKF	Madgwick	Mahony
Roll	5.05	5.54	5.87
Pitch	3.24	3.93	4.53
Yaw	5.93	6.27	6.66

Table 2. Dynamic RMSE with noisy measurements.

Fig. 5 reports the measured magnetic field in absence and presence of the disturbance showing the high noise level. Executing the slow trajectory in such condition, the algorithms exhibit a degradation of the performance as it can be appreciated in Fig. 6 and from the RMSE figures reported in Tab. 2.

As a further analysis, a comparison on the computational burden of the considered algorithms has been carried out. In particular, the algorithms have been implemented in Matlab/Simulink environment on an Intel I7 quad-core processor at 1.6 GHz. The tic-toc Matlab functions have been used to estimate the execution time of a single cycle that includes the gyroscope, accelerometer and magnetometer measurement and the attitude estimation. The

Algorithm	Matlab/Simulink [ms]	Embedded System [ms]
EKF	0.1	2.7
Madgwick	0.017	0.15
Mahony	0.014	0.11

Table 3. Computational burden estimation

superior performance of the EKF can be attributed to the availability of a tunable parameter for each sensor measurement, which is paid in terms of a higher execution time. Finally, to validate the proposed results, the algorithms have been coded for implementation on the STM32F3Discovery evaluation board using Chibi/OS as real-time embedded operating system. To this aim, the ARM Cortex Microcontroller Software Interface Standard (CMSIS) DSP library is used to implement the mathematical operations, i.e., matrix product and inverse. Table 3 reports the average time required to compute one estimation cycle in both Matlab/Simulink environment and embedded system implementation. Even though the execution times of the two fastest algorithms would allow to use a lower sampling time, this would lead to a negligible improvement due to the limited update rate of the magnetometer and gyroscope sensors.

6. CONCLUSION

An experimental comparison of popular IMU-based algorithms for orientation estimation of a rigid body with respect to a reference frame is presented in this work. In particular, two specifically designed solutions are compared to a standard EKF algorithm, which outperforms the others, as experimentally demonstrated, at the expense of a higher computational burden. However, its generality allows the user to add further sensory information without the need to completely re-design the estimation filter or to re-tune the parameters of the algorithm, which are simply based on the statistics of the noise affecting each measured signal.

REFERENCES

Bennett, C., Odom, C., and Ben-Asher, M. (2013). Knee angle estimation based on imu data and artificial neural networks. In *Biomedical Engineering Conf. (SBEC)*, 111–112.

Bischoff, R., Huggenberger, U., and Prassler, E. (2011). Kuka youbot - a mobile manipulator for research and education. In *IEEE Int. Conf. on Robotics and Automation (ICRA)*, 1–4.

Camps, F., Harasse, S., and Monin, A. (2009). Numerical calibration for 3-axis accelerometers and magnetometers. In *IEEE Int. Conf. on Electro/Information Technology*, 217–221.

Chen, S., Ding, C., Han, Y., Fang, Y., and Chen, Y. (2012). Study on information fusion algorithm for the miniature ahrs. In *4th Int. Conf. on Intelligent Human-Machine Systems and Cybernetics*, 114–117.

Crassidis, J.L., Markley, F.L., and Cheng, Y. (2007). A survey of nonlinear attitude estimation methods. *J. of Guidance, Control, and Dynamics*, 30, 12–28.

Falco, P., Maria, G.D., Natale, C., and Pirozzi, S. (2012). Data fusion based on optical technology for observation of human manipulation. *Int. J. of Optomechatronics*, 6, 37–70.

Gietzelt, M., Wolf, K.H., Marschollek, M., and Haux, R. (2013). Performance comparison of accelerometer calibration algorithms based on 3d-ellipsoid fitting methods. *Computer Methods and Programs in Biomedicine*, 3, 62–71.

Jingang, Y., Junjie, Z., Dezhen, S., and Jayasuriya, S. (2007). Imu-based localization and slip estimation for skid-steered mobile robots. In *IEEE/RSJ Int. Conf. on Intelligent Robots and Systems (IROS)*, 2845–2850.

Joong-hee, H., Kwon, J., Impyeong, L., and Kyoungah, C. (2011). Position and attitude determination for uav-based gps, imu and at without gcps. In *Int. Workshop on Multi-Platform/Multi-Sensor Remote Sensing and Mapping (M2RSM)*, 1–5.

Kim, H.S., Choi, H.S., su Yoon, J., and Ro, P. (2011). Study on ahrs sensor for unmanned underwater vehicle. *Int. J. of Ocean System Engineering*, 1, 165–170.

Madgwick, S., Harrison, A., and Vaidyanathan, R. (2011). Estimation of imu and marg orientation using a gradient descent algorithm. In *IEEE Int. Conf. on Rehabilitation Robotics (ICORR)*, 1–7.

Mahony, R., Hamel, T., and Pflimlin, J.M. (2008). Nonlinear complementary filters on the special orthogonal group. *IEEE Trans. on Automatic Control*, 53, 1203–1218.

Marins, J., Yun, X., Bachmann, E., McGhee, R., and Zyda, M. (2001). Extended kalman filter for quaternion-based orientation estimation using marg sensors. In *Proc. of the 2001 IEEE/RSJ Int. Conf. on Intelligent Robots and Systems*, 2003–2011.

Natale, C. (2011). Kinematic control of robots with noisy guidance system. In *Proc. of the 18th IFAC World Congress*, 6937–6944.

Pedley, M. (2013). High precision calibration of a three-axis accelerometer - an4399. Technical report, Freescale Semiconductor.

Prayudi, I. and Doik, K. (2012). Design and implementation of imu-based human arm motion capture system. In *Int. Conf. on Mechatronics and Automation (ICMA)*, 670–675.

Sabatini, A. (2006). Quaternion-based extended kalman filter for determining orientation by inertial and magnetic sensing. *IEEE Trans. on Biomedical Engineering*, 53, 1346–1356.

Xia, L., Wang, J., and Liu, Y. (2008). Quadratic ekf algorithm enhancements for low cost tightly-coupled ahrs/gps. In *2nd Int. Symposium on Systems and Control in Aerospace and Astronautics*, 1–6.

Zecca, M., Saito, K., Sessa, S., Bartolomeo, L., Lin, Z., Cosentino, S., Ishii, H., Ikai, T., and Takanishi, A. (2013). Use of an ultra-miniaturized imu-based motion capture system for objective evaluation and assessment of walking skills. In *35th Annual Int. Conf. of the IEEE Engineering in Medicine and Biology Society (EMBC)*, 4883–4886.

Ziegler, J., Kretzschmar, H., Stachniss, C., Grisetti, G., and Burgard, W. (2011). Accurate human motion capture in large areas by combining imu- and laser-based people tracking. In *IEEE/RSJ Int. Conf. on Intelligent Robots and Systems (IROS)*, 86–91.